Title

Silicic acid electrolyte additive reduces charge transfer impedance at sub-ambient temperature for lithium-ion rechargeable batteries

Authors

Fang, Chen
Tran, Thanh-Nhan
Ahmed, Faiz
et al.

Publication Date

2023-05-01

DOI

10.1016/j.elecom.2023.107489

Electrochemistry Communications 150 (2023) 107489

Contents lists available at ScienceDirect

Electrochemistry Communications

journal homepage: www.elsevier.com/locate/elecom

Silicic acid electrolyte additive reduces charge transfer impedance at sub-ambient temperature for lithium-ion rechargeable batteries

Chen Fang [a], Thanh-Nhan Tran [a,1], Faiz Ahmed [a], Dion Hubble [a], Yanbao Fu [a], Bryan D. McCloskey [a,b], Vincent S. Battaglia [a], Gao Liu [a,*]

[a] Energy Storage and Distributed Resources Division, Lawrence Berkeley National Laboratory, 1 Cyclotron Road, Berkeley, CA 94720, USA
[b] Department of Chemical and Biomolecular Engineering, University of California Berkeley, Berkeley, CA 94720 USA

ARTICLE INFO

Keywords:
Silicic Acid
Electrolyte Additive
Low Temperature
Lithium-ion Batteries
Solid Electrolyte Interphase

ABSTRACT

Vehicle electrification is a critical application of lithium-ion batteries (LIBs), and it is essential to develop LIBs that can operate at sub-ambient temperatures with satisfying performance. Conventional LIBs have performance deficits at low temperatures which hinder their use in extreme environments. One approach to address this problem is to rationally engineer the electrode/electrolyte interface with electrolyte additives to improve the electrochemical kinetics at sub-ambient temperatures. In this work, silicic acid (SiAc) is incorporated into standard LIB electrolyte as an additive to enhance the capacity and energy density of LIBs at temperatures down to −20 °C. Full-cell impedance analysis and X-ray photoelectron spectroscopy of cycled electrodes point towards an additive-induced change in surface chemistry which alters the charge transfer process. It is proposed that the SiAc additive participated in the formation of solid electrolyte interphase (SEI) and lowered the activation energy of the interface impedance, assisting lithium ion transport across the interface at lower temperatures.

1. Introduction

Lithium-ion batteries (LIBs) dominate most rechargeable energy storage applications and have allowed wide electrification of vehicles in recent years, which in turn generates a strong demand for higher energy output of LIBs in extreme environments, as one ubiquitous remaining problem for LIBs is their poor performance at sub-zero temperatures [1,2]. This deficit is caused by a rapid impedance rise with decreasing temperature, largely attributable to slower ion transport through the cell [3,4]. Although alternative lithium battery systems are available, such as lithium-air batteries [5–7] and lithium-sulfur batteries [8–10], LIBs still have wide applicability due to their stable performance, versatility, and plausibly high energy density with silicon-based anodes [11–14]. Generally speaking, the optimization of lithium battery systems has a range of topics from the battery material perspective, including binder [15–17], active materials [18–20], and electrolyte [21–23]. The engineering of electrolyte phase is a convenient approach to improve battery performance because it commonly has minor impact on battery configuration and fabrication [24,25]. The typical LIB electrolyte system contains lithium salts dissolved in carbonate solvents such as ethylene carbonate (EC), diethyl carbonate (DEC), dimethyl carbonate (DMC), and ethyl methyl carbonate (EMC), which have stable performance at ambient temperature [26–28]. As electrolyte is present at all internal cell surfaces and fills the spaces between them, it influences battery impedance *via* its bulk chemistry as well as its chemistry at the active material interface. Interfacial effects are primarily divided between charge transfer resistance and solid electrolyte interphase (SEI) resistance, which together make up the majority of internal resistance at room temperature and below [29]. At low temperatures such as −20 °C, LIBs have significantly lower discharge capacity that is practically due to the suppressed functionalities of the electrolyte solution, including reduced ionic conductivity and increased interfacial charge transfer impedance [30].

The ubiquity of electrolyte's influence throughout the cell means that any attempt to change one of these factors must necessarily consider its effect on other processes as well. This makes additive engineering an attractive tool for rational electrolyte design [31–33]. Applying a relatively low quantity of small-molecule additives to a liquid electrolyte system is a cost-efficient approach to enhance the performance of LIBs, including increase of cell cycle life [34], formation of protective films on

* Corresponding author.
E-mail address: gliu@lbl.gov (G. Liu).
[1] Present address: Energy and Environment Directorate, Pacific Northwest National Laboratory, Richland, WA 99354.

https://doi.org/10.1016/j.elecom.2023.107489
Received 15 February 2023; Received in revised form 2 April 2023; Accepted 5 April 2023
Available online 14 April 2023

electrodes [35,36], and flame retardancy of the electrolyte system [37,38]. In addition, inorganic materials can also be incorporated into electrolyte as additives for LIBs [39–41]. In gel polymer electrolyte (GPE) of LIBs, the incorporation of fumed silica has been found beneficial for improving ionic conductivity, where the Si–O bond of fumed silica could serve as a bridge and allow higher lithium ion transference [42]. The surface –OH groups of silica could be modified to host lithium salt moieties as a lithium ion source [43,44]. This type of lithium-modified silica could be applied as an additive to regular organic carbonate electrolytes of LIBs [45]. The electrolyte with lithium-silica additive exhibited superior high-rate capacity at −20 °C in a $LiCoO_2$/graphite cell. As for organic molecule additives for low temperature battery applications, fluoroethylene carbonate (FEC), tris(trimethylsilyl)phosphite, and sulfur-containing molecules have been found helpful in improving cell performance in cold environments [29].

In this study, we report a silicon-based inorganic additive, silicic acid (SiAc), in regular LIB electrolyte and its performance enhancement at sub-ambient temperatures. The effects of temperature and SiAc concentration were examined. In addition, the working mechanism of the SiAc additive was investigated. The SiAc additive has a minor impact on electrolyte composition but can significantly affect the interface behavior when the additive is incorporated into the SEI layer, especially at low temperatures.

2. Experimental section

2.1. Electrolyte formulation

Silicic acid (SiAc) is purchased from the Sigma-Aldrich chemical company. The baseline electrolyte is 1.0 M lithium hexafluorophosphate in ethylene carbonate/ethyl methyl carbonate 3/7 electrolyte (1.0 M $LiPF_6$ in EC/EMC 3/7 w/w) from Tomiyama Pure Chemical. The electrodes and electrolyte are acquired from the Argonne National Lab CAMP facility. Silicic acid is further dried at 60 °C under vacuum overnight. The electrolytes with 0.1%, 0.2%, 0.5%, 0.75%, and 1% silicic acid were formulated in an inert atmosphere glovebox by mixing the dried silicic acid powder with the electrolyte under magnetic stir for 12 h and were stored in sealed plastic bottles in the glove box.

2.2. Cell fabrication

The batteries were made with CR2032-type coin cell hardware (from Hohsen Corporation) using baseline electrolytes with/without SiAc additive. For each cell, a piece of Gr anode (91.83 wt%, ~ 3.16 mAh cm^{-2}), a piece of polypropylene separator (PP Celgard 2400) and a piece of single-side coated $LiNi_{0.6}Mn_{0.2}Co_{0.2}O_2$ cathode (NMC622, 90 wt%, ~ 2.56 mAh cm^{-2}) were sandwiched together with 40 uL electrolyte and crimped in coin cells inside the argon-filled glovebox. The graphite (Gr) and NMC622 electrodes were supplied by Argonne National Laboratory. All materials have been thoroughly dried before use.

2.3. Testing procedure

The electrochemical measurements were carried out on a Maccor 4200 system and Biologic VMP3 system. Activation and pre-cycling of the cells were performed at 30 °C with charge–discharge at C/20 rate for 3 cycles with cut-off voltage between 3.0 and 4.2 V, subsequently at C/10 rate for 3 cycles, at C/3 rate for 3 cycles, and 3 cycles at C/3 rate between 2.5 and 4.2 V. The cell performance at low temperatures was examined through a protocol as follows: (1) Charge-discharge cycling was performed at C/3 rate between 2.5 and 4.2 V for 4 cycles at 30 °C; (2) The cell was charged to 4.2 V at C/10 rate at 30 °C after resting for 3 h; (3) After changing the temperature to − 20 °C and then resting for 3 h, the cell was discharged to 2.5 V at a C/3 rate; (4) The step (3) was further repeated sequentially but at variable temperatures of −10, 0, 10, 20, and 30 °C. The overall cell specific capacity and cell energy density were calculated based on the cathode materials weight contents. The calculated cell energy numbers were only used for comparison among similar cells at different conditions. The charge–discharge cycling of the cells at 30 °C was performed with cut-off voltage between 2.5 and 4.2 V.

2.4. XPS characterization

The surface of the electrodes was analyzed by X-ray photoelectron spectroscopy (XPS) to better understand the impact of the additive. All of the cycled cathodes (NMC622) and anodes (graphite) (cells were stopped at discharge state) were soaked overnight in dimethyl carbonate (DMC) solvent and dried before XPS analysis. An air-free sample holder with Ag-tape on Si-substrate was kept inside the Ar-filled glove box and the electrodes were secured with the Ag-tape. The XPS analyses were performed using a Thermo-Fisher K-Alpha Plus XPS/UPS analyzer (operating pressure of 2.0 × 10–7 Pa) with a monochromatic Al Kα X-rays (1.486 eV) source at The Molecular Foundry.

3. Results and discussion

SiAc belongs to a group of silicate acids which takes a form of either single molecule or an oligomeric structure with Si-O bonds. The SiAc additive has limited solubility in the carbonate electrolytes (approx. 2% by weight). The baseline electrolyte for this study is 1.0 M $LiPF_6$ in EC/EMC 3/7 (w/w), which is a common type of electrolyte in LIBs [46–48]. A series of different SiAc weight ratios (0.1–1%) were examined. The low additive loading would hardly change the bulk electrolyte properties, and the additive's major functionality is to modify the interfacial properties between the electrode and electrolyte. This approach is focused on solving the interfacial challenges raised by the slow ion transportation and high resistivity in LIBs at low temperatures.

The electrolytes with SiAc additive concentrations ranging from 0.1% to 1.0% are used to evaluate the low temperature performance in a high energy Gr ‖ NMC622 lithium-ion cell configuration. The room temperature (30 °C) performances of the cells were first examined (Fig. 1). The cells with 0.1 to 0.5% SiAc additive show roughly identical performance at 30 °C compared to baseline-electrolyte cell. With higher additive concentration at 0.75 to 1%, the charge and discharge capacities at room temperature decreased by 5 to 6%, with higher concentration of SiAc additive leading to lower capacity (Fig. 1A). Additionally, the higher additive concentration resulted in a small increase in overpotential during both the charge and discharge processes compared to the baseline cell (Fig. 1B,C). It is plausible that excessive additive loading can cause detrimental effects [49,50], and further discussion of the impact of SiAc concentration is provided in later sections.

The variable temperature discharge test was performed to evaluate the impact of the SiAc additive at low temperatures (Fig. 2). The cells were charged at C/10 rate at 30 °C to reach full capacity, followed by cooling down to −20 °C and equilibrating for 3 h (cells in rest status). The cells were then discharged at a C/3 rate to 2.5 V as a cut off voltage and allowed to rest. The recorded energy and capacity are the cell performance at −20 °C. The cells were then warmed up to −10 °C and equilibrated for 3 h. The cell voltage climbed up during warming up and resting period, allowing the cells to discharge again at C/3 rate to 2.5 V. Such a discharging protocol was further repeated until reaching room temperature, raising 10 °C each time. The accumulated discharge energies of the cells were recorded over time (Fig. 2B). With this approach, the accumulated energy output at a given temperature might have slight deviation from the full discharge energy capacity, where the cell would be discharged at this single temperature point rather than across variable temperatures. But this method could provide accurate readings of cell performance at −20 °C, which is of the most interest, and can also provide credible performance comparison between cells with different additive concentrations. The results show that the SiAc additive provided both higher capacity and energy density during discharge at −20 °C at all additive concentrations (Fig. 2A,C). The cells with higher

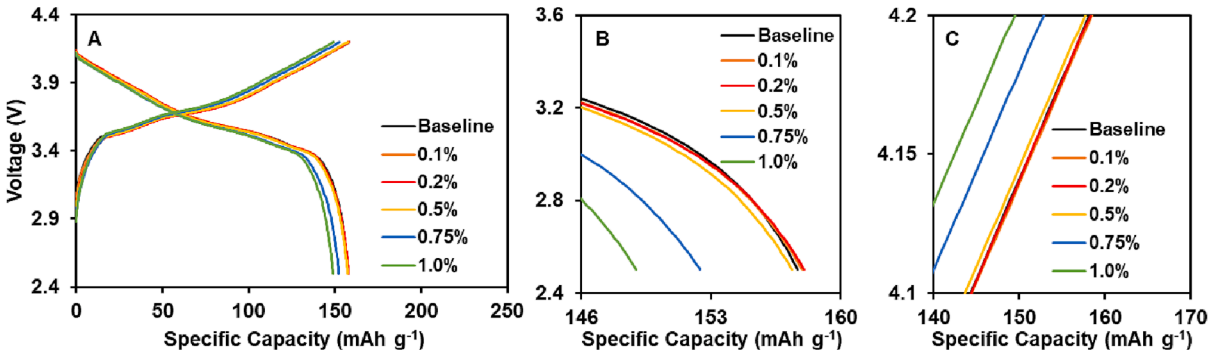

Fig. 1. Charge-discharge profiles of Gr || NMC622 coin cells with different SiAc additive concentrations in the 1.0 M $LiPF_6$ in EC/EMC 3/7 (w/w) at C/3 rate and 30 °C. A. Full charge and discharge profile at 3rd cycle between 2.5 and 4.2 V. B. Expanded region of the terminal section of discharging curves. C. Expanded region of the terminal section of charging curves.

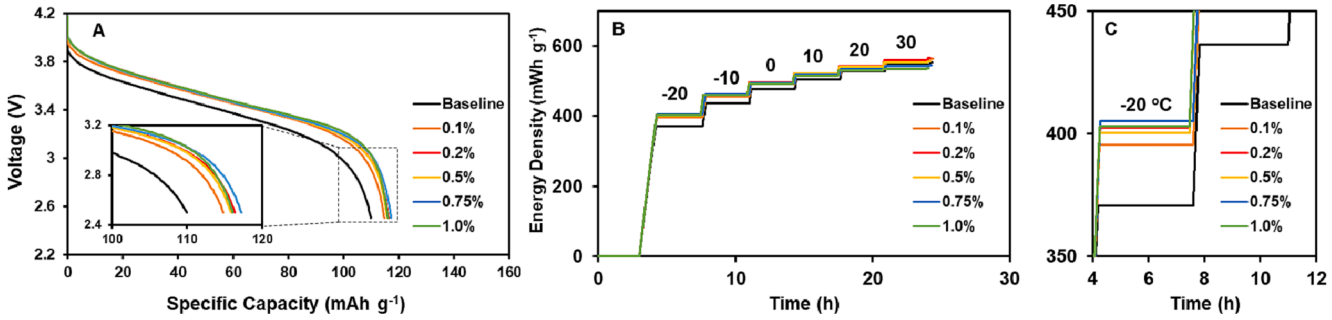

Fig. 2. Low-temperature discharge profiles of Gr || NMC622 cells with different SiAc concentrations in the 1.0 M $LiPF_6$ in EC/EMC 3/7 (w/w). A. Discharge capacity of cells at −20 °C (cells fully charged at 30 °C). B. Discharge energy density of cells at from −20 to 30 °C (plateaus reflect cell resting time with their heights corresponding to the accumulated discharge energy of the previous discharge steps). C. Expanded region of discharge energy density profile after initial discharge at −20 °C.

SiAc concentrations of 0.75 to 1.0 % perform better than the others with lower additive concentrations at −20 °C. However, higher additive concentration at both 0.75% and 1.0 % appreciably underperform the baseline cells at 30 °C. The lower additive concentration at 0.1 to 0.5% had both outstanding cell performance improvement at low temperature and equivalent performance to the baseline cell at ambient temperature.

Energy density performances of the cells with different SiAc additive loadings are summarized in Fig. 3, which is the performance of the cells at −20 °C compared to that of baseline cell at 30 °C. At the temperature of −20 °C, 0.75% SiAc gives the best performance that is 6 percentage points higher in energy density retention than baseline electrolyte. Although 0.75 to 1.0 % SiAc concentration yields the best relative low temperature performance at −20 °C, their ambient-temperature capacity is appreciably lower than the baseline electrolyte. Consequently, the high SiAc loading of 0.75 to 1.0 % would not be the preferred concentration. Among the lower SiAc concentrations, namely 0.1 to 0.5%, the 0.2% additive loading led to highest energy density retention at −20 °C, which is 70.6%. Considering that 0.2% SiAc has negligible negative impact on cell capacity at ambient condition, it is the optimum choice of additive concentration.

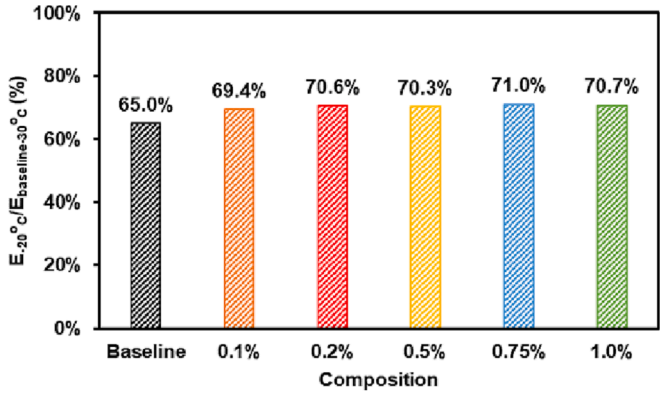

Fig. 3. Discharge energy density of cells with different SiAc concentrations at −20 °C compared to baseline cell at 30 °C.

Since less than 1.0 % SiAc additive was incorporated into the electrolyte, the difference of bulk electrolyte properties with varied additive loadings could be considered neglectable. Therefore, the performance enhancement at low temperatures was mainly a result of interface improvement realized by the SiAc additive. Electrochemical impedance spectroscopy (Fig. 4) and X-ray photoelectron spectroscopy (XPS, Fig. 5) were used to investigate the interface properties and the chemical changes at the SEI layer. The impedance measurements were performed with full cells at 50 % depth of discharge (DOD) without distinguishing the impacts on anode and cathode, as the additive was found incorporated in both cathode and anode interfaces (see discussions below).

Typically, two pseudo semi-circle can be observed by impedance spectroscopy for LIB cells. The lower frequency semi-circle is attributed to charge transfer impedance at both electrodes, and the higher frequency one is attributed to the SEI impedance of the two electrodes [51,52]. As shown in Fig. 4A, a low SiAc concentration of 0.2% did not outstandingly alter the impedance of the cell when compared to the baseline electrolyte, whereas a higher additive concertation of 0.75% pushes up both SEI and charge transfer impedances. These results are consistent with the cell capacity retention and overpotential behavior at 30 °C in Fig. 1. As shown in Fig. 4B,C, when the temperature is decreased to 0 and −20 °C, the impact of temperature on SEI resistance (*i.e.* higher-frequency semi-circle) is small for all the cells, but is significant on charge transfer impedance (*i.e.* lower-frequency semi-circle) of the cells.

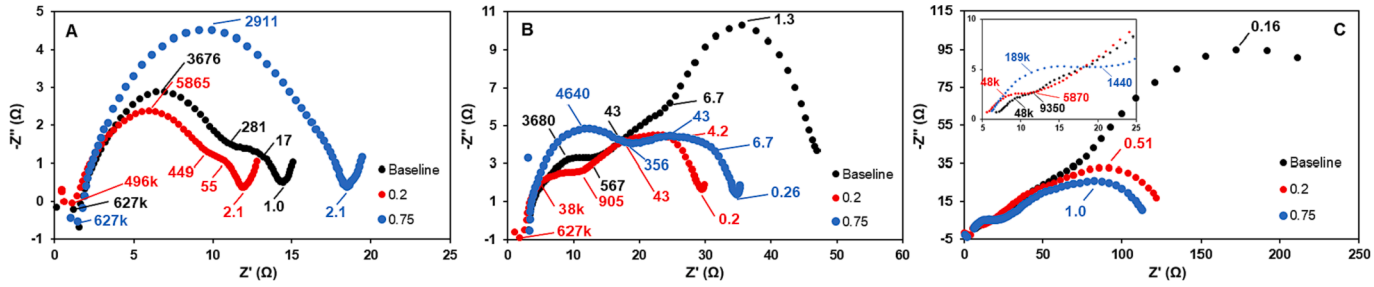

Fig. 4. The variable temperature impedance of the baseline cell and SiAc-containing cells at 50% DOD. The positions and frequencies are labeled by line and numbers on the graphs. A. 30 °C. B. 0 °C. C. −20 °C, insert is the expanded high-frequency region.

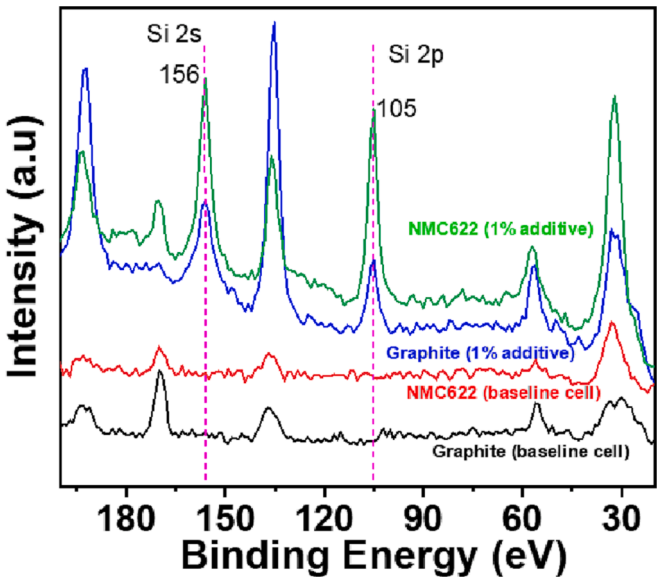

Fig. 5. XPS of the graphite and NMC electrode surfaces with dotted vertical line labeling the positions of Si s and p signals (electron binding energy at 155 and 105 eV respectively).

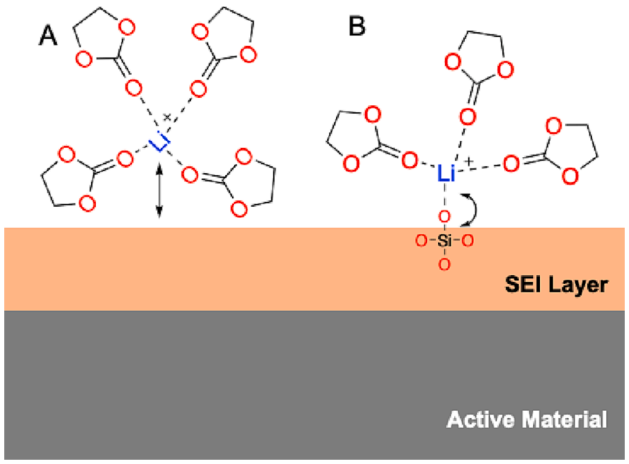

Fig. 6. The solvation of Li ion at the interface of the SEI and electrolyte, and Li ion charge transfer mechanisms at the SEI surface. A. Without Si-O functionality at the surface of SEI layer. B. The Si-O at the surface of SEI can assist the Li ion solvation/de-solvation.

As the bulk electrolyte does not change much at 0.2 to 1.0 % additive concentration, it is reasonable to conclude that the charge transfer is impacted by a difference in chemistry in the SEI layer. In particular, the charge transfer impedance of the baseline cell grows significantly at lower temperatures. The introduction of SiAc additive at 0.2 and 0.75% concentration both can lower the impedance but the difference between these two concentrations is not dramatic. From Fig. 4, it can be suggested that a high SiAc loading at 0.75% might be most helpful for reducing the cell impedance at −20 °C, but a lower SiAc loading at 0.2% could be more favored for 0 and 30 °C. This is caused by the different interface chemistry enabled by the SiAc additive, which is discussed below.

The XPS analyses (Fig. 5) confirmed the integration of the Si-O species into the SEI layer as strong Si *s* and *p* orbital electron signals [53] are observed from both the surfaces of cathode and anode that were cycled with the SiAc additive. Due to the formation of the four Si-O bonds on one Si atom, the *p* orbital electron energy shifted to a much higher position of around 105 eV, confirming the integration of the Si-O component in both cathode and anode instead of the reduced form of Si species in the anode. It is interesting to note that a higher concentration of Si-O species in the SEI layer improves the low temperature performance, but increases the impedance at ambient temperature. Since the SiAc component might be integrated in the SEI layer, we hypothesize that the surface Si-O species may participate in the charge transfer step as shown in the schematics in Fig. 6. The Si-O bond that participates in the charge transfer step may be less temperature sensitive, and therefore, in the low temperature range, it appears to facilitate charge transfer. But at ambient temperature, this pathway appears to be more resistive. Similar situations can be found in solid state electrolytes (SSEs), where the conductivity of SSE slightly decreases as the temperature goes to sub-ambient [54,55]. The existence of a high concentration of the Si-O sites in SEI layers may increase the impedance of Li ion transport at ambient or higher temperatures. Therefore, a balanced concentration of SiAc additive in electrolyte at the lower end of its possible range leads to formation of less dense Si-O sites, which preserves the ambient and high temperature performance. The impact of SiAc additive on room temperature (30 °C) cell cycling performance is demonstrated in Fig. S1. The SiAc additive did not negatively impact the cell rate performance (Fig. S1a), and did not present unfavorable influence on long cycling performance (Fig. S1b). Therefore, it can be concluded that SiAc additive would not outstandingly deteriorate the battery's room temperature cycling stability and rate capability.

4. Conclusions

The fact that a low SiAc additive concentration of 0.2% can produce appreciable energy gain at −20 °C without outstanding negative effects in a standard lithium-ion rechargeable battery electrolyte system is nothing short of remarkable. This study is focused on the interfacial aspects of low temperature cell performance. The SiAc additive is incorporated into the SEI layer. Although a high SiAc loading can decrease the combined charge transfer impedance and the SEI resistance at low temperatures, it can raise the impedance at ambient conditions. Therefore, a moderate additive concentration would be the optimum choice. Under low-temperature conditions, the energy density gain is a

result of the lowered interface impedance of the SiAc modified interface, primarily coming from the reduction of the charge transfer impedance component of the EIS.

CRediT authorship contribution statement

Chen Fang: Conceptualization, Formal analysis. **Thanh-Nhan Tran:** Conceptualization, Data curation, Formal analysis. **Faiz Ahmed:** Data curation, Formal analysis. **Dion Hubble:** Data curation, Formal analysis. **Yanbao Fu:** Formal analysis. **Bryan D. McCloskey:** Supervision, Formal analysis. **Vincent S. Battaglia:** Supervision, Formal analysis. **Gao Liu:** Conceptualization, Supervision, Formal analysis.

Declaration of Competing Interest

The authors declare that they have no known competing financial interests or personal relationships that could have appeared to influence the work reported in this paper.

Data availability

Data will be made available on request.

Acknowledgement

This research was supported by the Assistant Secretary for Energy Efficiency, Vehicle Technologies Office of the U.S. Department of Energy (DOE). X-ray photoelectron spectroscopy (XPS) was performed at The Molecular Foundry of Lawrence Berkeley National Laboratory. Work at the Molecular Foundry was supported by the Office of Science, Office of Basic Energy Sciences, of the U.S. Department of Energy under Contract No. DE-AC02-05CH11231.

Appendix A. Supplementary data

Supplementary data to this article can be found online at https://doi.org/10.1016/j.elecom.2023.107489.

References

[1] A. Gupta, A. Manthiram, Advanced Energy Materials 10 (2020) 2001972.
[2] G. Zhu, et al., Journal of Power Sources 300 (2015) 29–40.
[3] D. Zhang, et al., Energy Reports 8 (2022) 4525–4534.
[4] P. Mei, et al., Nanoscale 15 (2023) 987–997, https://doi.org/10.1039/D2NR06294A.
[5] X. Chi, et al., Nature 592 (2021) 551–557.
[6] C. Wang, et al., Energy Storage Materials 43 (2021) 221–228.
[7] Z. Guo, et al., Advanced Functional Materials 32 (2022) 2108993.
[8] C. Fang, et al., APL Materials 7 (2019), 080902.
[9] Z. Li, et al., ACS Applied Polymer Materials 1 (2019) 1965–1970.
[10] Z. Liu, et al., Advanced Functional Materials 30 (2020) 2003605.
[11] D. Larcher, J.M. Tarascon, Nature Chemistry 7 (2015) 19–29.
[12] J.D. McBrayer, et al., Nature Energy 6 (2021) 866–872.
[13] X. Jiang, et al., Carbon 191 (2022) 448–470.
[14] M.C. Schulze, et al., Journal of The Electrochemical Society 169 (2022), 050531.
[15] J. Kim, et al., Chemistry of Materials 34 (2022) 5791–5798.
[16] Z. Liu, et al., ACS Applied Materials & Interfaces 13 (2021) 46518–46525.
[17] P. Parikh, et al., Chemistry of Materials 31 (2019) 2535–2544.
[18] J. Kou, et al., ACS Applied Materials & Interfaces 7 (2015) 17910–17918.
[19] S. Zhou, et al., Carbon Energy 2 (2020) 143–150.
[20] S. Zhou, et al., Batteries & Supercaps 4 (2021) 240–247.
[21] X. Fan, et al., Nature Energy 4 (2019) 882–890.
[22] R. Petibon, et al., Electrochimica Acta 154 (2015) 227–234.
[23] X. Ma, et al., Electrochimica Acta 270 (2018) 215–223.
[24] X. Ma, et al., Journal of The Electrochemical Society 164 (2017) A3556.
[25] Y. Zhao, et al., Frontiers in Chemistry 8 (2020), 484, https://doi.org/10.3389/fchem.2020.00484.
[26] S.V. Sazhin, et al., Journal of Power Sources 87 (2000) 112–117.
[27] C. Fang, et al., Journal of The Electrochemical Society 167 (2020), 020506.
[28] C. Fang, et al., Electrochimica Acta 399 (2021), 139362.
[29] D. Hubble, et al., Energy & Environmental Science 15 (2022) 550–578.
[30] N. Zhang, et al., Advanced Materials 34 (2022) 2107899.
[31] G. Song, et al., ACS Applied Materials & Interfaces 13 (2021) 40042–40052.
[32] C. Fang, et al., Joule 5 (2021) 415–428.
[33] J. Shi, et al., Journal of Power Sources 429 (2019) 67–74.
[34] L. Liao, et al., Electrochimica Acta 87 (2013) 466–472.
[35] S. Grugeon, et al., Journal of Power Sources 427 (2019) 77–84.
[36] E.J. Hopkins, et al., Journal of The Electrochemical Society 168 (2021), 030534.
[37] S. Chen, et al., Journal of Power Sources 187 (2009) 229–232.
[38] E.-G. Shim, et al., Electrochimica Acta 54 (2009) 2276–2283.
[39] B. Wu, et al., RSC Advances 4 (2014) 10196–10203.
[40] B. Wu, et al., Solid State Ionics 260 (2014) 8–14.
[41] S. Komaba, et al., Journal of Power Sources 119–121 (2003) 378–382.
[42] Y. Liao, et al., Electrochimica Acta 54 (2009) 6396–6402.
[43] N.-S. Choi, et al., Solid State Ionics 167 (2004) 293–299.
[44] J. Sun, et al., Electrochimica Acta 52 (2007) 7083–7090.
[45] L. Hamenu, et al., Current Applied Physics 16 (2016) 611–617.
[46] M. Raghibi, et al., Electrochimica Acta 362 (2020), 137214.
[47] T. Zhu, et al., Journal of Power Sources 521 (2022), 230889.
[48] C. Fang, et al., ACS Applied Energy Materials 5 (2022) 11655–11661.
[49] B. Liu, et al., ACS Applied Materials & Interfaces 11 (2019) 21496–21505.
[50] L. Liao, et al., Solid State Ionics 254 (2014) 27–31.
[51] S.S. Zhang, et al., Electrochimica Acta 49 (2004) 1057–1061.
[52] H. Xiao, et al., APL Materials 10 (2022), 011108.
[53] S.C. Ray, et al., Journal of Applied Physics 118 (2015), 115302.
[54] T. Kwon, et al., ACS Applied Materials & Interfaces 9 (2017) 24250–24258.
[55] Z. Lin, J. Liu, RSC Advances 9 (2019) 34601–34606.